



Cite this: *Soft Matter*, 2019,
15, 289

Hierarchical modelling of polystyrene melts: from soft blobs to atomistic resolution

Guojie Zhang, ^{ab} Anthony Chazirakis, ^{cd} Vagelis A. Harmandaris, ^{*cd} Torsten Stuehn, ^b Kostas Ch. Daoulas ^{*b} and Kurt Kremer ^{*b}

We demonstrate that hierarchical backmapping strategies incorporating generic blob-based models can equilibrate melts of high-molecular-weight polymers, described with chemically specific, atomistic models. The central idea is first to represent polymers by chains of large soft blobs (spheres) and efficiently equilibrate the melt on large scales. Then, the degrees of freedom of more detailed models are reinserted step by step. The procedure terminates when the atomistic description is reached. Reinsertions are feasible computationally because the fine-grained melt must be re-equilibrated only locally. We consider polystyrene (PS) which is sufficiently complex to serve method development because of stereo-chemistry and bulky side groups. Our backmapping strategy bridges mesoscopic and atomistic scales by incorporating a blob-based, a moderately coarse-grained (CG), and a united-atom model of PS. We demonstrate that the generic blob-based model can be parameterised to reproduce the mesoscale properties of a specific polymer – here PS. The moderately CG model captures stereo-chemistry. To perform backmapping we improve and adjust several fine-graining techniques. We prove equilibration of backmapped PS melts by comparing their structural and conformational properties with reference data from smaller systems, equilibrated with less efficient methods.

Received 7th September 2018,
Accepted 27th November 2018

DOI: 10.1039/c8sm01830h

rsc.li/soft-matter-journal

1 Introduction

A molecular structure based understanding of properties of technologically or experimentally relevant polymer melts, or dense solutions, still poses significant scientific challenges. Computational studies of structure–process–property relationships in polymer liquids often require the consideration of atomistic details, while at the same time many fundamental scientific questions and important technological applications can be addressed only for high molecular-weight (MW) polymers. These simultaneous requirements create major challenges at high polymer concentrations, *e.g.* concentrated solutions and melts. For typical polymerisation degrees in industrial applications, the average spatial extension of random-walk-like chains lies¹ between 10 and 100 nm. In concentrated polymer liquids these fractal “threads” strongly interdigitate. To avoid finite-system

size effects, simulations must consider samples with dimensions that are at least two times larger than the root-mean-square end-to-end distance of the molecules, R_e . This minimum requirement, however, already leads to samples that contain hundreds or even thousands of polymers, which easily corresponds to many millions of atomistic degrees of freedom.

To demonstrate that samples spanning only a couple of R_e have a large number of particles, it is useful to consider the following scaling estimate.^{2,3} The number of polymers crossing the volume of a test chain is proportional to $\sqrt{N} = (n/V)R_e^3$, where n and V are, respectively, the total number of chains and volume of the system. In polymer melts $R_e^2 \simeq N_k l_k^2$, where N_k is the number of Kuhn segments in a chain and l_k the length of a single Kuhn segment. The chain density is expressed through the volume per single Kuhn segment, v_k , as $n/V = 1/v_k N_k$. Therefore $\sqrt{N} = l_k^3 \sqrt{N_k} / v_k$. Because v_k / l_k^2 defines the packing length p , $l_k^3 / v_k = l_k / p$. l_k / p plays a key role for rheological properties and for many polymers⁴ $l_k / p \sim 1\text{--}10$. Since the molecular mass of a Kuhn segment is typically a few hundred g mol⁻¹, for polymers with high MW⁵ $N_k \sim 10^3$ and thus $\sqrt{N} \sim 10^2$. In other words, simulations of melts with long chains must handle samples where the basic subvolume, $\sim R_e^3$, already contains one hundred chains (at least). The overlapping polymers are strongly entangled⁶ and their relaxation times are prohibitively long. Their equilibration with atomistic molecular dynamics (MD) is unfeasible even when

^a Institute for Systems Rheology, Advanced Institute of Engineering Science for Intelligent Manufacturing, Guangzhou University, 510006 Guangzhou, China. E-mail: guojie.zhang@gzhu.edu.cn

^b Max Planck Institute for Polymer Research, Ackermannweg 10, 55128 Mainz, Germany. E-mail: daoulas@mpip-mainz.mpg.de, kremer@mpip-mainz.mpg.de

^c Department of Mathematics and Applied Mathematics, University of Crete, GR-71409 Heraklion, Crete, Greece. E-mail: harman@uoc.gr

^d Institute of Applied and Computational Mathematics, IACM/FORTH, Heraklion, Greece



using massively parallel simulations. Therefore approaches circumventing the slow relaxation path of physical dynamics are of significant interest. Well equilibrated atomistic systems are indispensable initial conditions to simulation studies of atomistic long-chain polymer melts. Various strategies are available, including advanced connectivity altering Monte Carlo (MC) algorithms^{7,8} and methods based on hierarchical multiscale modelling.

Hierarchical multiscale modelling involves multiple scales of description^{9–17} and offers a powerful concept for tackling large system sizes and protracted equilibration times. The central idea is to benefit from scale separation: in polymers long-wavelength behavior often follows universal laws¹⁸ that incorporate chemistry-specific information into a few parameters. Therefore, one can initially eliminate microscopic features hampering equilibration and prepare samples reproducing only mesoscopic conformational and structural properties. These samples serve as “blueprints” for reinserting the missing microscopic features without disturbing long-wavelength properties. The reinsertion is computationally feasible because only local re-equilibration is required. Two major strategies realise this idea: configuration assembly and hierarchical backmapping.

Configuration assembly^{14,19–22} algorithms construct the initial sample by putting together polymer chains under a fixed average density. Implementations vary in details, but in all cases chains are generated to reproduce prescribed distributions of conformations. If the ensemble is generated as an ideal gas of chains, important long-wavelength structural properties, such as the correlation hole effect,¹⁸ are missing. Therefore, one must reduce the large density fluctuations of the ideal gas of chains and introduce some interchain correlations through chain packing schemes.^{19,20} Subsequently local conformations and liquid packing are recovered through a “push off” procedure, which gradually¹⁹ reinserts the microscopic excluded volume into the ensemble. The strategy has been successful with generic^{19,20} and chemistry specific^{14,21,22} microscopic models. However, the postulative construction of starting configurations is a drawback. The assumption that polymers have ideal random-walk-like conformations in melts is only approximately true.^{23,24} Examples of deviations from ideal random-walk statistics are found in the power-law decay of bond–bond correlations²³ and statistics of polymer knots.²⁵ Predicting conformations for polymers with complex architecture (star-like or branched) and systems that are inhomogeneous or multicomponent is even less straightforward. Furthermore, the computational costs at the stage of chain packing increase with molecular weight.

Hierarchical backmapping is a more general approach, taking advantage of a general concept originating from renormalization group theory in critical phenomena. The material is described at several “nested” length scales, introducing a sequence of coarse-grained (CG) models. The sequence is terminated by the microscopic model. Because the sample is equilibrated at the largest length scale with standard simulations (handling the crudest CG model), long-wavelength properties are not postulated but follow from a rigorous statistical-mechanical framework. The molecular details resolved by the next model are reinserted through local

sampling of configuration space. Repeating the procedure, one descends the hierarchy of models, step by step, until the microscopic description is reached. The efficiency increases significantly^{22,26–31} when the hierarchy includes soft models, *i.e.* models where the strength of non-bonded interactions is comparable to the thermal energy.

Blob-based models^{27,32–47} offer a straightforward way to construct hierarchies of CG representations: N_b monomers of a microscopically-resolved subchain are lumped into a single soft blob (sphere), so that polymers are represented by chains of blobs. Varying N_b generates a family of models with different resolutions. Hierarchical backmapping using blob-based models has been successful in equilibrating high-molecular-weight polymer melts^{27,47} and blends⁴⁸ described with generic (bead-spring like) microscopic models. The equilibrated samples typically contained 10^3 chains, comprised of a few thousands of beads. The method is not limited to these examples – the computational costs of the procedure are not affected by chain length and are, roughly, proportional only to the volume of the system.²⁷ Yet, the question of whether hierarchical strategies with blob-based models can equilibrate melts described with chemically-specific atomistic models remains, so far, open. Concerns regarding this point have been expressed in the literature.²²

Here we address this question and demonstrate that hierarchical strategies with generic blob-based models can equilibrate melts of actual polymers, described with chemically-specific atomistic models. As an illustration we develop a hierarchical backmapping method which equilibrates large atomistically-resolved samples of polystyrene (PS) melts. PS is a basic commodity material and is well-suited for method development: it is well studied experimentally and theoretically, and is a sufficiently complex polymer, where molecules have tacticity and bulky units (benzene rings). To descent the hierarchy of scales, from coarse to atomistic, our backmapping strategy incorporates a blob-based,^{39,43} a moderately^{49,50} CG, and a united-atom^{49,51} (UA) model of PS. We demonstrate that a generic blob-based model^{39,43,47} can describe the rather complex PS melt accurately enough to allow backmapping. To perform backmapping within the hierarchy of chemically-specific models, we improve and adjust several reinsertion techniques.^{14,19,20} These methodological issues are also discussed in the paper.

2 Hierarchy of models

Our hierarchical strategy for equilibrating large samples of high-molecular-weight polymer melts, described with atomistic detail, requires several models covering a broad range of length scales: from atomistic, to moderately CG, up to mesoscopic. In this section we present the models used for the hierarchical description of PS.

2.1 Atomistic model

On the atomistic level we describe PS through a united atom (UA) model based on the TraPPE-UA force field.⁵² Details can be



found in previous studies,^{49,51,53} so we mention here briefly that in this UA model each PS monomer is represented by groups of eight UAs (see Fig. 1(a)). The full interaction potential of atomistic PS involves bonded and non-bonded terms. Angular and torsional potentials are introduced for the aliphatic backbone, while keeping the lengths of the bonds fixed. Improper dihedral potentials are used to keep the phenyl ring planar and to maintain the tetrahedral configuration around the sp^3 -hybridised carbon connected to the phenyl ring. Non-bonded interactions between UAs are captured by pairwise Lennard-Jones (LJ) potentials.

Despite the fact that we are using a UA model, it is rather straightforward to obtain and simulate all-atom systems by adding hydrogens to the UA PS configurations. However, since the chosen UA PS model has been extensively used and examined before, we choose to represent the atomistic PS chains in the UA description.

2.2 Moderately coarse-grained model

We employ a moderately (quantitative) CG model that has been derived^{14,53} from the UA description presented in Section 2.1. The model and the procedure used to obtain the CG force field have been elaborated elsewhere.^{14,49} In summary, each PS monomer is mapped on two effective beads, “superatoms”, A and B (see Fig. 1(b)). Bead A represents the CH_2 unit of a PS monomer and half of each of the two neighboring CH groups along the chain backbone. Bead B stands for the phenyl ring. The sizes and masses of A and B superatoms are $\sigma_A = 4.1 \text{ \AA}$, $\sigma_B = 5.2 \text{ \AA}$, $m_A = 27 \text{ amu}$, and $m_B = 77 \text{ amu}$, respectively. Such a model is capable of providing quantitative predictions about both static and dynamic properties of PS systems. In addition, for the moderately CG model we define: (a) a characteristic length scale as the average bead size, *i.e.*, $\sigma_{CG} = (\sigma_A + \sigma_B)/2 = 4.65 \text{ \AA}$, and (b) a characteristic time scale, $\tau = \sqrt{m_A \sigma_{CG}^2 / k_B T}$ ($k_B T$ is the thermal energy).

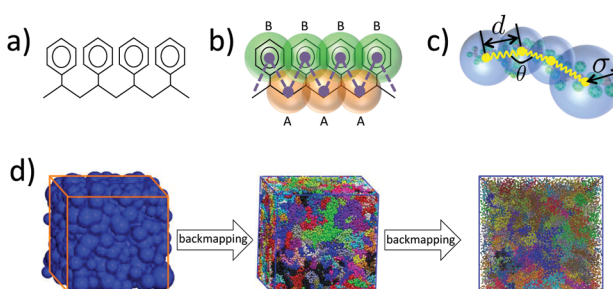


Fig. 1 PS models used during hierarchical backmapping: (a) the united atom (UA) model; (b) the moderately coarse-grained (CG) model, A-type beads (orange) represent a CH_2 group and half of its two neighboring CH groups along the aliphatic backbone, while B-type beads (green) describe the phenyl rings; and (c) the blob-based (BL) model constructed by grouping a large number of beads of the moderately CG model into soft spheres. (d) Summary of basic steps of the hierarchical backmapping. An equilibrated blob-based configuration of PS is first obtained from efficient Monte Carlo (MC) simulations and the degrees of freedom of the moderately CG model are reinserted into this configuration. The equilibrated PS melt obtained after this reinsertion is further backmapped on the UA description. The snapshots show an equilibrated PS melt with 100 chains and 480 monomers per chain (MW = 50 kDa) at three different resolutions.

This CG scheme can describe tacticity of PS chains without introducing side groups, by classifying the B beads into four subtypes. In total, the bonded part of the CG force field includes one bond, but four “alternative” angular and dihedral interaction potentials. The specific sequence of potentials chosen for angular and dihedral interactions along the backbone of a moderately CG chain depends on the tacticity of the atomistic PS molecule it represents.

Nonbonded interactions are described through pair LJ-like, $n-m$ potentials $U_{\alpha,\beta}(r)$, where r is the distance between two interacting superatoms. The powers and parameters used in $U_{\alpha,\beta}(r)$ depend on the type α and β of the interacting superatoms, *i.e.* a bead can be A type or belong to one of the four B types. Non-bonded interactions are deactivated for those beads that belong to the same chain and are closer neighbours than (1,5). The details and the parameters of the force-field can be found elsewhere.^{14,53}

The accuracy of the moderately CG model in predicting quantitatively the properties of PS melts has been verified through extensive investigations.^{14,53} Moreover it was recently demonstrated⁵⁴ that the moderately CG model is transferable to the crystalline phase of syndiotactic PS. Specifically, it reproduces the crystallisation temperature and stabilises the main α and β polymorphs. For the purposes of our backmapping scheme, the fine structure of the CG model presents significant advantages because it facilitates the subsequent reinsertion of the degrees of freedom of the UA description.

2.3 Blob-based coarse-grained model

2.3.1 Model description. A moderately CG polystyrene molecule with N_{CG} superatoms is represented by a sequence of $N_{BL} = N_{CG}/N_b$ spheres (blobs). As illustrated in Fig. 1(c), each blob stands for a PS subchain with N_b superatoms, so that the choice of N_b determines the resolution of the drastically CG description. The radius σ_i and the coordinates of the center of the i -th sphere, \mathbf{r}_i , match (respectively) the instantaneous gyration radius, $R_{g,i}$, and the position of the center-of-mass (COM), $\mathbf{R}_{cm,i}$, of the underlying PS subchain.

The connectivity of soft-sphere chains is described^{32,39,40,43} using bond, V_b , and angular, V_θ , potentials, defined as:

$$\beta V_b(d) = \frac{3d^2}{2b_{BL}^2} \text{ and } \beta V_\theta(\theta) = \frac{1}{2}k_{BL}(1 + \cos \theta), \quad (1)$$

where d and θ are the distance and angle between consecutive spheres and bonds in a soft-sphere chain, respectively. The parameters b_{BL} and k_{BL} control the strength of the potentials; their energy scale is expressed in units of $k_B T$ ($\beta = 1/k_B T$).

The fluctuations of the radius, σ , of a sphere are controlled by a “self-interaction” potential, $V_s(\sigma)$, similar to the Flory free energy.⁵⁵ This potential is defined as:

$$\beta V_s(\sigma) = c_1 \frac{\sigma^2}{N_b} + c_2 \frac{N_b^2}{\sigma^3} \quad (2)$$

The first term in eqn (2) has entropic origin and balances the swelling induced by the second term, which implicitly accounts for binary intramolecular interactions between the

N_b superatoms underlying the blob. In previous studies^{27,39,43,47} the interactions controlling the fluctuations of σ were augmented by a term proportional to $1/\sigma^6$ (following Lhuillier⁵⁶). In the first implementation of the soft-sphere model³⁹ the $1/\sigma^6$ term enabled the description of a broad range of concentration regimes, *e.g.* dilute solutions. However, in melts the $1/\sigma^6$ term is significantly smaller than the $1/\sigma^3$ term⁵⁷ and thus can be omitted.

The effective non-bonded interactions between two spheres, i and j , are described by a Gaussian potential:

$$\beta V_{\text{nb}}(r_{ij}) = \varepsilon N_b^2 \left(\frac{3}{2\pi\bar{\sigma}^2} \right)^{3/2} \exp\left(-\frac{3r_{ij}^2}{2\bar{\sigma}^2}\right) \quad (3)$$

where r_{ij} is the distance between the centers of the spheres, $\bar{\sigma}^2 = \sigma_i^2 + \sigma_j^2$, and ε controls the strength of repulsion.⁵⁸ $\beta V_{\text{nb}}(r_{ij})$ is obtained by approximating the interactions of superatoms underlying different spheres by binary repulsive collisions and is proportional to the overlap of two Gaussian clouds. Each of these clouds describes the average distribution in space of superatoms with respect to the COM of the subchain they belong to.

The soft-sphere model of the PS is motivated by simple arguments from polymer physics. The model aims to capture long-wavelength conformational and structural properties of PS melts accurately enough for performing backmapping at one state point. In this work, we define state points using the density of the blobs $\rho_{\text{blob}} = nN_{\text{BL}}/V$ and temperature T . Due to the simple Gaussian-potential approximation used for the non-bonded interactions, we do not expect that various thermodynamic properties of polystyrene, *e.g.* the equation-of-state, can be well approximated within our soft-sphere model, on the level of the blob description. The reinsertion of atomistic details corrects the thermodynamic inconsistencies.

To sample the configurational space of PS melts described with the soft-sphere model, we benefit from an efficient Monte Carlo (MC) algorithm based on three types of moves: (i) random change of sphere size, (ii) random sphere displacement, and (iii) slithering snake (reptation). A detailed presentation of the method can be found elsewhere.⁴³ We summarise that the computational efficiency stems from a special particle-to-mesh calculation of nonbonded interactions, which avoids neighbor lists.^{27,43}

2.3.2 Parameterisation strategy. The first step is to set the resolution of the soft-sphere model by choosing N_b . At least formally, pairwise non-bonded potentials as in eqn (3) are only an approximation^{42,45,59} to actual multibody potentials of mean force (PMF) between blobs in the underlying (microscopic) polymeric system. For some theoretical frameworks, *e.g.* integral equation theory, the accuracy of this approximation is still under discussion.^{60,61} In blob-based models pairwise potentials can be turned into an accurate description of the actual PMF by choosing^{44,45} N_b such that the blob size is smaller than the Edwards correlation length ξ . This condition ensures that the blobs defined in the actual system are “dilute”. Consequently, the PMF of the microscopic system can be accurately reproduced by the coarse-grained pairwise potentials. The approach is well

suited for polymer solutions because ξ increases as the polymer concentration decreases. In polymer melts, however, ξ is microscopic and the ansatz with the “diluted” blobs is expected to fail.⁴⁵ In this case N_b should be chosen to be “sufficiently large” because of two reasons. First, assuming that the conformations of the chains in the melt have approximately^{23,24} random-walk statistics, choosing large N_b justifies³² the use of eqn (1) for bonded potentials. Second, large N_b are necessary for softening the effective interactions between blobs. Previous studies^{27,59} have demonstrated that the Gaussian potential of non-bonded interactions, eqn (3), can be parameterised in this regime to reproduce the blob–blob pair correlation function $g(r)$ in melts with sufficient accuracy for successful backmapping.²⁷ We emphasise that for such N_b values the Gaussian potential is only an approximation of the actual multibody PMF; their difference can be quite large.⁵⁹ The thermodynamic inconsistencies in the melts of soft-sphere chains obtained using this approximate potential are corrected only after backmapping.

At the same time, N_b must be smaller than the entanglement length, N_e , for the final backmapping step. When soft-sphere chains are substituted by the moderately CG polymers, the liquid structure and chain conformations in the melt must be relaxed on scales smaller or comparable to the average blob diameter. The condition $N_b < N_e$ warrants that this relaxation is achieved through fast Rouse-like dynamics of short subchains and is not affected by surrounding topological constraints.²⁷ Had we employed a hierarchy with several blob-based models,²⁷ the condition $N_b < N_e$ would apply only to the last, highest resolution, blob-based model (where the reinsertion of the moderately CG description is performed). Depending on the method used to extract the entanglement length, simulations of PS have reported N_e in the range of 100–200 monomers, which is equivalent to 200–400 superatoms.⁴⁹ These results agree with experiments.^{62–64} Therefore, we explore different resolutions satisfying the condition $N_b \leq 200$. The entanglement time in the moderately CG model is $\tau_e \simeq 4 \times 10^4 \tau$.

For each trial N_b , the parameters c_1 , c_2 , b_{BL} , k_{BL} , and ε are determined using typical structure-based (or Inverse Boltzmann) coarse-graining.^{9,13,65} The parameters are chosen so that the probability distributions $P_{\text{BL}}(\sigma)$, $P_{\text{BL}}(d)$, and $P_{\text{BL}}(\theta)$, as well as the pair-correlation function, $g_{\text{BL}}(r)$, of the centers of the spheres in blob-based PS melts reproduce closely their counterparts in reference samples described by the moderately CG model. These reference samples contain 50 chains with $N_{\text{CG}} = 960$ superatoms and were equilibrated through a variant¹⁴ of the configuration-assembly method proposed by Auhl *et al.*¹⁹ and long CG molecular dynamics simulations. The density of chains in the reference samples is $n/V = 1.17 \times 10^{-2}$ chains per nm³ and the temperature is set to $T = 463$ K. In the moderately CG reference samples, the polymers are partitioned into subchains with N_b superatoms. The length of the chains in the reference samples restricts the N_b that can be considered here to a limited set of values, to have an integer number of subchains, *i.e.* under the condition $N_b \leq 200$, we try $N_b = 192, 160, 120$, and so on. After the subchains are identified, we calculate the distributions of: (i) the gyration radii of subchains, $P_{\text{ref,BL}}(R_g)$; (ii) the distance



between the COMs of subchains sequential in the same PS molecule, $P_{\text{ref,BL}}(d)$; and (iii) the angles between two vectors joining the COM of a subchain with the COMs of the preceding and the succeeding subchain, $P_{\text{ref,BL}}(\theta)$ (cf. Fig. 1(c)). The pair distribution function of the COMs of subchains, $g_{\text{ref,BL}}(r)$, serves as the counterpart of $g_{\text{BL}}(r)$.

With the reference distributions in hand, the parameters of the soft-sphere model are optimised through an iterative procedure which simultaneously minimises four merit functions, defined⁶⁶ as:

$$\Delta_{f(x)} = \int_0^{x_{\text{cutoff}}} w(x) [f(x) - f_{\text{ref}}(x)]^2 dx, \quad (4)$$

where $f(x) = P_{\text{BL}}(\sigma)$, $P_{\text{BL}}(d)$, $P_{\text{BL}}(\theta)$ and $g_{\text{BL}}(r)$; $f_{\text{ref}}(x)$ is the corresponding reference function. In this study, we set the weighting function $w(x)$ in eqn (4) to a constant, $w(x) = 1/x_{\text{cutoff}}$, so that it has no effect on $\Delta_{f(x)}$. For $P_{\text{BL}}(\theta)$ no cutoff is required, since $\theta \in [0, \pi]$. For $f(x) = P_{\text{BL}}(\sigma)$ and $P_{\text{BL}}(d)$, the x_{cutoff} is chosen such that $f(x_{\text{cutoff}}) \simeq 10^{-4}$. We use $x_{\text{cutoff}} = 12\sigma_{\text{CG}}$ for $f(x) = g_{\text{BL}}(r)$, because $g_{\text{ref,BL}}(r = 12\sigma_{\text{CG}})$ saturates, within the noise of the data, to unity.

To start the iterative procedure, the initial values of b_{BL} and k_{BL} are obtained by fitting the Boltzmann distributions of the potentials $V_b(d)$ and $V_\theta(\theta)$ from eqn (1) to the reference distributions $P_{\text{ref,BL}}(d)$ and $P_{\text{ref,BL}}(\theta)$, respectively. The parameters c_1 and c_2 are obtained in a similar way by fitting the Boltzmann distribution of the potential $V_s(\sigma)$, eqn (2), to $P_{\text{ref,BL}}(R_g)$. We emphasise that this first estimate of the parameters is approximate, because it assumes that the distributions are not correlated. A first-guess value for ε can be obtained from c_2 . To first order, the two parameters can be related to each other by equating the potential $c_2 N_b^2 / \sigma^3$ (cf. eqn (2)), which captures the effect of the repulsion between intramolecular superatoms, to the “self-interaction” of a Gaussian density distribution. The latter is given by $\beta V_{\text{nb}}(0)/2$; the prefactor 1/2 avoids double counting. This approximation leads to $c_2 = (\varepsilon/2)(3/4\pi)^{3/2}$.

To perform the first iteration step, cf. Fig. 2, we consider the soft-sphere model with the initial values of parameters. The number of blobs in the soft-sphere chains equals the number of subchains used to partition the moderately CG molecules in the reference samples. The melt has $n = 100$ soft-sphere chains and the volume is chosen such that n/V matches the chain density in the reference systems. The temperature does not appear explicitly in the soft-sphere model, because all interactions in eqn (1) and (2) are scaled by the thermal energy. The melt is equilibrated using particle-to-mesh MC and the distribution function $P_{\text{BL}}(\sigma)$ is extracted to calculate $\Delta_{P_{\text{BL}}(\sigma)}$. The parameters c_1 and c_2 are increased or decreased by 5% and a new simulation is performed. The procedure is repeated until $\Delta_{P_{\text{BL}}(\sigma)}$ reaches a minimum value. The configurations from the simulation with the last optimised c_1 and c_2 are used to calculate $\Delta_{P_{\text{BL}}(d)}$. The parameter b_{BL} is modified until $\Delta_{P_{\text{BL}}(d)}$ reaches a minimum. The same procedure is repeated for k_{BL} and ε ; the corresponding merit functions are $\Delta_{P_{\text{BL}}(\theta)}$ and $\Delta_{g_{\text{BL}}(r)}$, cf. Fig. 2. After updating all parameters, we commence a new iteration step. We recalculate $\Delta_{P_{\text{BL}}(\sigma)}$ and improve c_1 and c_2 by minimising again $\Delta_{P_{\text{BL}}(\sigma)}$. Subsequently, the remaining parameters are improved, as in

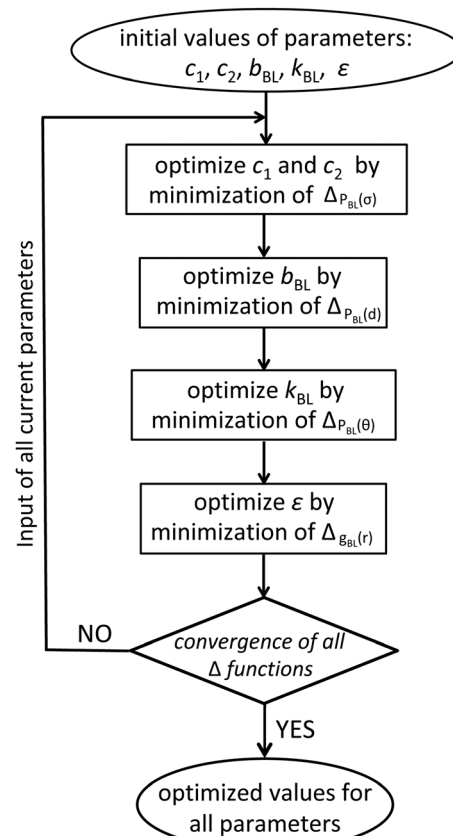


Fig. 2 Procedure used to parameterise the blob-based model of polystyrene melts.

the first iteration step. Iteration steps are repeated (e.g. by about five circles in our case) until the minimum values of all merit functions, $\Delta_{f(x)}$, saturate.

Through exploratory studies we find that the simple soft-sphere model can be parameterised to reproduce static properties of the reference PS melt when $N_b \gtrsim 120$. Backmapping a soft-sphere model with the smallest possible N_b is preferable, because this procedure requires shorter relaxation times of reinserted microscopic details. Therefore, in this study we work with $N_b = 120$; that is, each blob corresponds to 120 CG superatoms or 60 PS monomers.

2.4 Validation of the soft-sphere model

We illustrate that the melts equilibrated with the soft-sphere model indeed describe structural and conformational properties of PS melts on length scales comparable to or larger than the size of the blobs. For $N_b = 120$, the four panels of Fig. 3 present the distributions $P_{\text{BL}}(\sigma)$, $P_{\text{BL}}(d)$, and $P_{\text{BL}}(\theta)$, as well as the pair distribution function, $g_{\text{BL}}(r)$, for a melt of soft-sphere chains (lines) and reference samples (symbols). The agreement of the curves is remarkable. As will be demonstrated in the following, the small deviations observed in the plots do not propagate into the properties of backmapped PS samples.

Fig. 4(a) and (b) examine the accuracy of the soft-sphere model on scales comparable to the size of the entire PS chain.

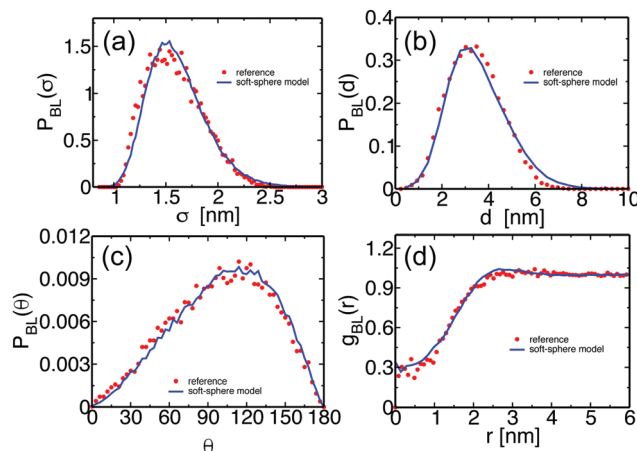


Fig. 3 For a PS melt of soft-sphere chains corresponding to $N_b = 120$, the lines show the probability distributions of (a) the sphere radius, σ , (b) the bond length, d , between spheres, and (c) the angle, θ , between successive bonds. The reference distributions calculated for moderately CG melts of PS are plotted with symbols. (d) For the same melt, the pair distribution function $g_{BL}(r)$ of the centers of the soft spheres (lines) is compared with the pair distribution of the COMs of the subchains with $N_b = 120$ superatoms (symbols).

Fig. 4(a) presents for the soft-sphere model (lines) and reference samples (symbols) the intermolecular part $g_{inter,BL}(r)$ of the pair distribution functions plotted in Fig. 3(d). In both curves, the correlation holes of subchains (evident depletion at small distances) and of entire PS chains (shallow depletion towards tails) can be identified. The two $g_{inter,BL}(r)$ match each other closely, even in their long tails, demonstrating that the blob-based model captures the melt structure on large scales.

To compare polymer conformations in melts described by the soft-sphere and moderately CG models we employ the internal distance plot, which is a very sensitive conformational descriptor.¹⁹ Its general definition for a system containing n_c chains, each with N repeat units, reads:⁶⁷

$$C(m) \equiv \frac{R^2(m)}{m} \text{ where} \\ 0 < m < N, R^2(m) \equiv \left\langle \frac{1}{n_c(N-m)} \sum_{i=1}^{n_c} \sum_{j=1}^{N-m} [\mathbf{r}(i,j) - \mathbf{r}(i,j+m)]^2 \right\rangle \quad (5)$$

In eqn (5), $\mathbf{r}(i,j)$ stands for the position vector of the j -th repeat unit of the i -th chain and angular brackets denote an average over system configurations. The parameter m stands for the “chemical distance” of two repeat units on the same chain, *i.e.* it expresses the number of repeat units comprising the chain contour between the two considered units. The general definitions of $R^2(m)$ and m in eqn (5) are adjusted to the considered chain model. In the soft-sphere model, $R^2(s) \equiv R_{BL}^2(s)$ is the mean-square distance between the centers of two spheres in the same chain; $m \equiv s$ is the number of spheres between these two blobs along the chain contour. To compare the soft-sphere model with reference data, in our specific case, $R_{BL}^2(s)$ in moderately CG melts is defined as the mean-square

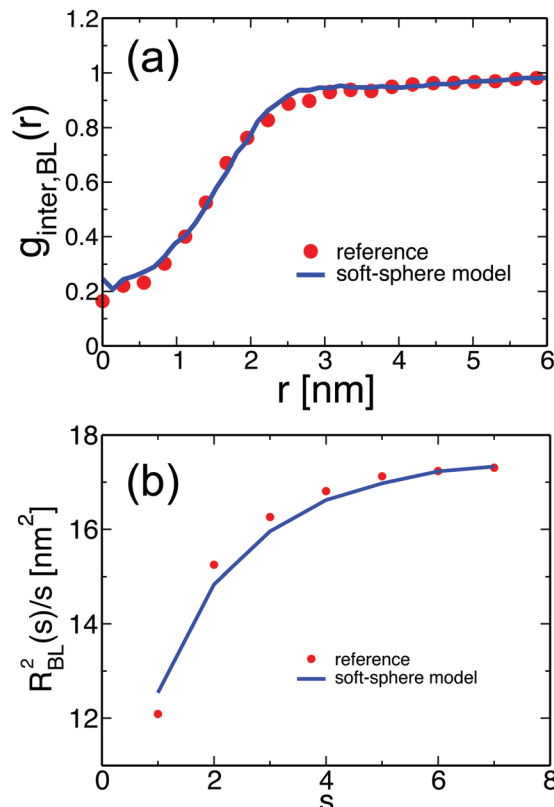


Fig. 4 (a) The line shows the intermolecular part, $g_{inter,BL}(r)$, of the pair distribution function of the centers of the blobs in PS melts of soft-sphere chains, corresponding to $N_b = 120$. Symbols present $g_{inter,BL}(r)$ of COMs of subchains with $N_b = 120$ superatoms, calculated from the reference samples of moderately CG melts of PS. (b) A normalised internal distance plot, $R_{BL}^2(s)/s$, calculated for PS melts of soft-sphere chains corresponding to $N_b = 120$ is shown with a line. Symbols present the internal distance plot calculated for the COMs of subchains with $N_b = 120$ superatoms in the reference samples.

distance between the COMs of two subchains with $N_b = 120$ superatoms, belonging to the same molecule. s is the number of intramolecular subchains between them. Fig. 4(b) compares $R_{BL}^2(s)/s$ in PS melts described by the soft-sphere (lines) and moderately CG (symbols) models. For large s the plots follow each other closely; for blobs, located near each other along the chain, the relative deviation is at most 3.7%. The internal distance plot demonstrates the accuracy of the soft-sphere model in describing conformational properties on the scale of entire chains.

3 Hierarchical backmapping strategy

3.1 Systems studied

The hierarchical scheme described in the previous section can be applied to systems of any molecular weight for a given density. In practice, for fixed pressure and temperature, the density of the polystyrene becomes chain-length independent for polymerisation degrees larger than about 50–100 monomers.⁴⁹ Therefore we expect that the soft-sphere model, developed in the previous section,



is transferable to PS melts with arbitrarily long chains. However, for the purposes of method development, we set here as a goal the equilibration of atomistic PS melts comprised of $n = 100$ chains with $N = 480$ repeat units, which corresponds to a molecular weight of $M = 50$ kDa. These molecules are equivalent to moderately CG PS molecules with $N_{\text{CG}} = 960$ superatoms and soft-sphere chains with $N_{\text{BL}} = 8$ blobs each. These are the chain lengths for which the soft-sphere model is parameterised and for which reference samples are available¹⁴ (cf. Section 2.3.2). Having the same chain lengths in backmapped and reference samples simplifies the validation of the equilibration. The temperature in the backmapped and reference melts is $T = 463$ K, which is a typical processing temperature for PS.

3.2 Backmapping the blob-based model to the chemically specific coarse-grained model

The reinsertion of the degrees of freedom of the chemically specific CG model into equilibrated soft-sphere PS melts is conceptually similar to the strategy developed earlier²⁷ for generic microscopic (bead-spring) models. Technically, however, the backmapping of the chemically specific CG model is more involved, due to the more complex CG force field. The technicalities of the different backmapping steps are presented below.

Introducing moderately CG PS molecules: every soft-sphere chain in the melt is replaced by a moderately CG PS molecule in a matching conformation. Specifically, the COM and the radius of gyration (squared) of each subchain with N_{b} superatoms in the reinserted molecule must match the COM and the radius (squared) of the corresponding blob in the soft-sphere chain. We generate each moderately CG PS molecule in the vicinity of the blob-based chain it must replace (the exact location is not critical). Setting the first bead of a generated molecule to A type, the remaining beads are added stepwise. A and B beads alternate. In this work, we assign randomly to each B bead one of the four subtypes (cf. Section 2.2) to make PS chains atactic. The length, bond angle, and torsional angle of the bond connecting the added superatoms to the part of the molecule that has been already constructed are randomly drawn from Boltzmann distributions. Each distribution depends on the appropriate bonded potential. Once the PS molecules are generated, we associate²⁷ with each subchain two external potentials: $\beta V_{\text{cm},i} = k_{\text{cm}}(\mathbf{r}_i - \mathbf{R}_{\text{cm},i})^2$ and $\beta V_{\text{g},i} = k_g(\sigma_i^2 - R_{\text{g},i}^2)^2$. Here $\mathbf{R}_{\text{cm},i}$ and $R_{\text{g},i}$ are the COM and squared radius of gyration of the i -th reinserted subchain, respectively. These potentials affect all superatoms in the i -th subchain, because $\mathbf{R}_{\text{cm},i}$ and $R_{\text{g},i}$ depend on the coordinates of all these superatoms. The parameters controlling the strength of the external potentials are empirically set to $k_{\text{cm}} = 100k_{\text{B}}T/\sigma_{\text{CG}}^2$ and $k_g = 100k_{\text{B}}T/\sigma_{\text{CG}}^4$. With the external and bonded potentials simultaneously activated (non-bonded potentials are turned off), the configuration of generated moderately CG molecules is subjected to *NVT* MD simulation, using the Langevin thermostat. This simulation “drives” every molecule into the corresponding soft-sphere chain. At this stage the molecules do not interact with each other, therefore the simulation takes negligible time.

Recovering the microscopic excluded volume: after the soft-sphere chains are replaced by the moderately CG PS molecules,

we remove the external potentials and gradually activate²⁷ the non-bonded interactions between superatoms. For this purpose we use a “push-off” MD procedure^{19,20} which removes overlaps between reinserted superatoms and recovers the original excluded volume characterising the potentials $U_{\alpha,\beta}(r)$. We summarise here the main features of the push-off protocol; details are provided in the Appendix.

The potentials are “force-capped” according to the rule:

$$U_{\alpha,\beta}^{\text{fc}}(r) = \begin{cases} (r - r_{\text{c}(n)}) U_{\alpha,\beta}'(r_{\text{c}(n)}) + U_{\alpha,\beta}(r_{\text{c}(n)}), & r \leq r_{\text{c}(n)} \\ U_{\alpha,\beta}(r), & \text{otherwise} \end{cases} \quad (6)$$

Here $r_{\text{c}(n)}$ is the force-capping radius and the original interactions are recovered when $r_{\text{c}(n)} \rightarrow 0$. The push-off is accomplished in 100 cycles; each of them comprises a change in $r_{\text{c}(n)}$ and local relaxation through a short MD simulation. For those beads that are not intramolecular (1,5) neighbours, we decrease $r_{\text{c}(n)}$ by a small step at the beginning of each cycle. For intramolecular (1,5) neighbours, $r_{\text{c}(1,5)}$ is adjusted in a special way in order to avoid significant distortions of polymer conformations during the push-off. To modify $r_{\text{c}(1,5)}$ in the beginning of each cycle, we use an approach similar to the one developed for generic microscopic models.²⁰ Namely, we quantify conformational distortions using the descriptor:

$$I = \int_{n_1}^{n_2} \left[\frac{R_{\text{CG}}^2(l)}{l} - \frac{R_{\text{CG,ref}}^2(l)}{l} \right] dl, \quad (7)$$

where $R_{\text{CG}}^2(l)/l$ is the internal distance plot calculated for the PS melt after the previous cycle of push-off is accomplished. The reference internal distance plot, $R_{\text{CG,ref}}^2(l)/l$, is obtained from the reference samples of moderately CG PS melts. The boundaries in l are empirically set to $n_1 = 50$ and $n_2 = 250$. We increase or decrease $r_{\text{c}(1,5)}$, depending on whether I is positive or negative.

The MD push-off procedure lasts about $20\tau_e$ which is a negligible fraction of τ_e , about 0.05%. In practice, this run takes less than a day on 32 processors of a typical supercomputer.

Local re-equilibration: once the excluded-volume interactions are recovered, the moderately CG PS melt is locally re-equilibrated through a standard MD simulation, which lasts about one τ_e . This is the most computationally demanding part of our procedure. To give a feeling for the CPU resources that are typically required for re-equilibration, we mention that it takes about 32 days using the ESPResSo++ package⁶⁸ (version 1.9.5) on 256 Xeon cores with a frequency of 3.0 GHz. We observe that the local re-equilibration of PS melts for $\sim \tau_e$ is about an order of magnitude slower – in terms of the required CPU time – compared to melts described with generic microscopic bead-spring models.²⁷ The protracted computations are not related to the backmapping strategy but are due to the complexity of the chemically-specific force-field. Because the largest relaxation time is determined by τ_e , the CPU time required by our backmapping procedure does not depend on chain length and is proportional only to system volume.²⁷ In contrast, the relaxation time in brute-force MD simulations is proportional to the reptation time, given by $\tau_{\text{rep}} \simeq \tau_e(N/N_e)^3$;

to make a simple scaling argument we use the approximate cubic power law of the initial reptation theory.^{6,69} The moderately CG PS melts considered here are only weakly entangled: based on the largest reported value $N_e = 400$ (cf. Section 2.3.2) we obtain $N/N_e \simeq 2.4$. The estimate for τ_{rep} demonstrates that to equilibrate even this system, brute-force MD simulations would require about a year of continuous running (using the same number of processors). Melts with slightly longer PS chains are entirely out of reach of brute-force MD simulations.

3.3 Validating backmapping of the moderately coarse-grained PS melts

We demonstrate the equilibration of backmapped moderately CG melts of PS by monitoring characteristic conformational and structural properties on local and global length scales. These properties are compared with their counterparts calculated for the reference samples. As a first simple test, we present in Fig. 5(a) and (b) the probability distributions of the bond angle and the torsional angle, $P_{\text{CG}}(\theta)$ and $P_{\text{CG}}(\phi)$. The data obtained for the backmapped melts (lines) are on top of the distributions (symbols) calculated for the reference samples.

The structure of the polymer liquid is quantified in Fig. 6(a) and (b), presenting the total, $g_{\text{CG}}(r)$, and the interchain, $g_{\text{inter,CG}}(r)$, pair-distribution functions of superatoms in the backmapped (lines) and reference (symbols) samples. The plots obtained for backmapped and reference systems are indistinguishable from each other. The agreement between $g_{\text{inter,CG}}(r)$ is particularly important; thanks to the correlation-hole effect¹⁸ this quantity is a sensitive quantifier of the mesoscopic liquid

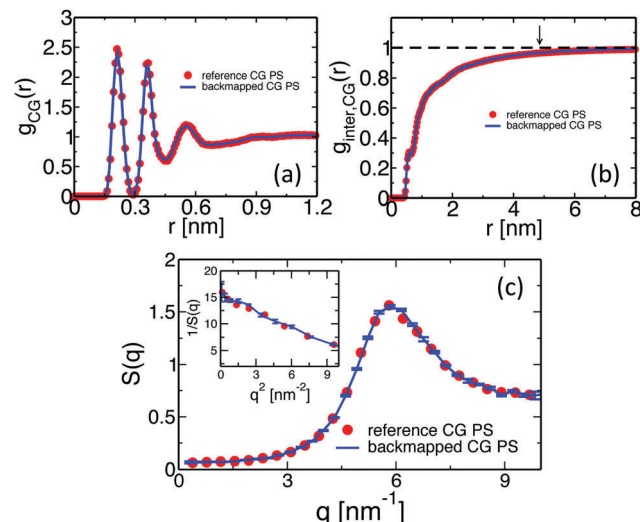


Fig. 6 Comparison of (a) total, $g_{\text{CG}}(r)$, and (b) intermolecular, $g_{\text{inter,CG}}(r)$, pair-distribution functions calculated for the backmapped (lines) and ref. 14 (symbols) CG melts of PS. Panel (c) shows the structure factor of density fluctuations in the backmapped (lines) and reference (symbols) melts. The inset presents the behavior of $1/S(q)$ for $q \rightarrow 0$, used to extract the isothermal compressibility.

structure on length scales comparable to the average size of the entire chain. The characteristic size of the correlation hole, defined by the average radius of gyration of the chains, is marked in Fig. 6(b) by the arrow. To illustrate more clearly that the backmapped melts reproduce correctly the long-wavelength density fluctuations of PS, we compare in Fig. 6(c) their static structure factor $S(q)$ (line) with its counterpart (symbols) for reference samples. The two plots agree with each other within the statistical noise of the data. The latter is quantified *via* the error bars, corresponding to the standard deviation calculated from four independent backmapped CG melts of PS. From the data in Fig. 6, we obtain the isothermal compressibility, κ_T , of atactic polystyrene at 463 K: $\kappa_T = S(q \rightarrow 0)/\rho k_B T \approx 8.7 \times 10^{-10} \text{ Pa}^{-1}$. Here ρ denotes the number density of superatoms in the CG PS configurations. The κ_T characterising the backmapped samples is remarkably close to $\kappa_T = 8.4 \times 10^{-10} \text{ Pa}^{-1}$ that has been experimentally reported for PS at 473 K.⁷⁰

One of the most stringent tests of equilibration is performed in Fig. 7, where we present the internal distance plot $R_{\text{CG}}^2(l)/l$ calculated for the backmapped (line) and reference (symbols) CG PS melts. The error-bars correspond to the 95% confidence interval and, for clarity, are shown only for the plot obtained from the backmapped melts. The error-bars grow at the tail of the plot due to fewer data available for calculating $R_{\text{CG}}^2(l)/l$. Within the noise of the data, the two plots match each other well and confirm the equilibration of the PS melts.

3.4 Backmapping from the chemically specific coarse-grained model to the atomistic model

In the following we describe the methodology for the backmapping from the moderately (chemically specific) CG scale to the atomistic one. Note that several different methods for

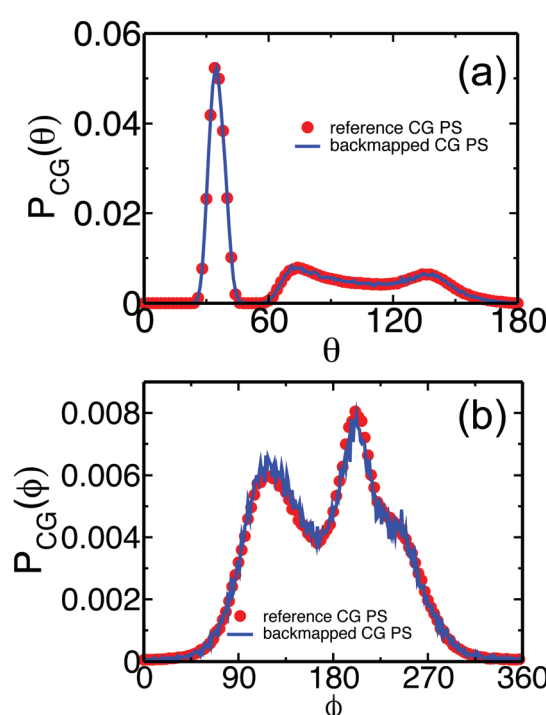


Fig. 5 Comparison of probability distributions of (a) bond angles, $P_{\text{CG}}(\theta)$, and (b) torsional angles, $P_{\text{CG}}(\phi)$, calculated for the backmapped (lines) and ref. 14 and 53 (symbols) CG melts of PS.



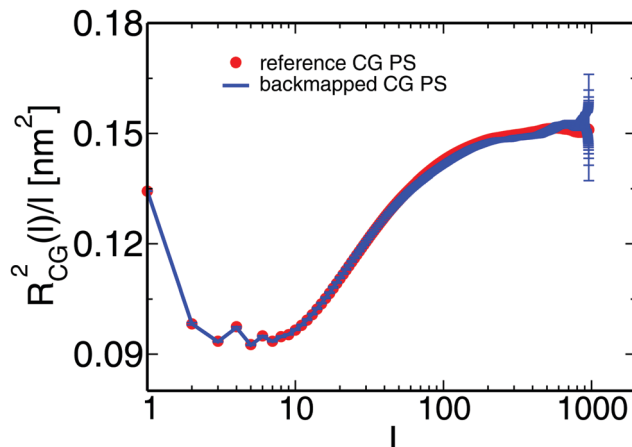


Fig. 7 The line and the symbols present, respectively, the internal distance plots calculated for backmapped and ref. 14 CG melts of PS.

re-introducing atomistic detail to CG polymer chain conformations have appeared in the literature.^{13,17,21,53,71,72}

Here, inspired by the above works, we propose a generic approach that is based on “lego-like” construction of consecutive monomers along a macromolecular chain. The backmapping algorithm is presented below.

Development of a CG “lego”-particle database: given a specific CG mapping scheme for PS chains, atomistic information about each CG particle is required. To obtain such information atomistic configurations of short PS chains are analysed. More specifically, a particle database (a set of “lego” classes), based on the chosen CG mapping scheme, is constructed including two types of information: first, each type of class represents a CG particle type and holds the atoms that define it, along with their relative positions, their masses and their contributing weights on the CG particle. In the specific CG PS model two different CG types are defined: one that describes the CG bead type “A” and one for the CG bead type “B”. The constructed A and B “legos” that correspond to the specific CG PS model are shown in Fig. 8(a). Note that lego A consists of a CH₂ and two

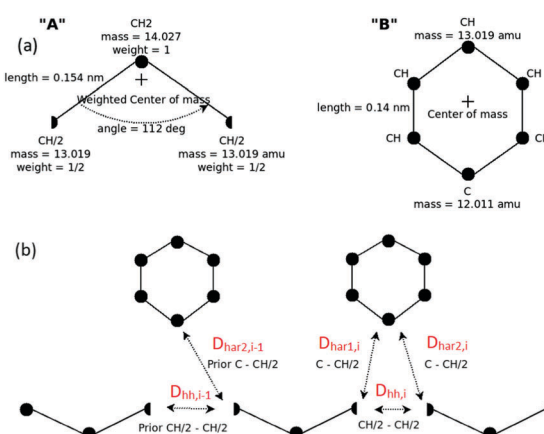


Fig. 8 (a) “Legos” that correspond to “A” and “B” CG groups. (b) Geometric re-introduction of the atomistic detail of two consecutive PS monomers along the CG PS configurations.

half CH groups, whereas lego B consists of the phenyl ring (five CH and one C groups).

Second, from the analysis of the atomistic configurations, additional information is gathered about: (a) the average and the distribution of distances between two consecutive CG particles (“AB” and “BA” CG bonds) and (b) the average and the distribution of angles between three consecutive CG particles (“ABA” and “BAB” CG angles).

Re-introduction of atomistic detail using a geometric algorithm: in the next stage, given the CG PS configurations obtained from the backmapping of the blob-based to the chemically specific CG representation, the atomistic ones are created. This is achieved *via* a geometric algorithm, by putting each “lego” piece at the given center-of-mass of its corresponding CG particle in a consecutive way. To avoid high overlaps the “legos” are rotated around their center-of-masses, to minimise distances between neighboring atoms; see Fig. 8(b).

In more detail, for a specific PS monomer i we define $D_{\text{hh},i}$ as the distance between the two CH halves, which correspond to the same CH united-atom group, and $D_{\text{har1},i}$ and $D_{\text{har2},i}$ the distances between the two halves and the “C” carbon of the aromatic ring, in the i th monomer.

In addition we define $\theta_{A,i} = [\theta_{A,x,i}, \theta_{A,y,i}, \theta_{A,z,i}]$ and $\theta_{B,i} = [\theta_{B,x,i}, \theta_{B,y,i}, \theta_{B,z,i}]$ as the three (Eulerian) rotation angles of the A and B CG particle-“lego” of the i th monomer, respectively. Based on the above we propose, along two consecutive PS monomers, the following minimisation problem:

$$\min_{\theta_{A,i}, \theta_{B,i}, \theta_{A,i+1}} F_{\text{cost}} \quad (8)$$

where the cost function is defined as:

$$F_{\text{cost}} = D_{\text{hh},i}^2 + w_1((D_{\text{har1},i} - D_{\text{har}})^2 + (D_{\text{har2},i} - D_{\text{har}})^2) + w_2(D_{\text{bh},i-1}^2 + (D_{\text{har2},i-1} - D_{\text{har}})^2) \quad (9)$$

where $D_{\text{har}} = 0.151$ nm is the (average) atomistic “C-backbone”–“C-aromatic” bond length. w_1 and w_2 are weights with typical values $w_1 = w_2 = 0.7$. Then, we minimise F_{cost} over all possible angles $\theta_{A,i}$, $\theta_{B,i}$, and $\theta_{A,i+1}$ via a BFGS method. This is a very fast minimisation procedure, since it involves information on only two consecutive monomers.

The above procedure is repeated for all pairs of consecutive monomers along the PS chain, in order to obtain a first realistic PS atomistic configuration.

Energy minimisation: the re-insertion of the atomistic detail on the CG PS configurations has been extensively tested and no strong overlaps between neighboring atoms were observed. However, due to possible correlations among the CG intramolecular (bonds, angles, and dihedrals) degrees of freedom, as well as due to the fact that the geometric method does not involve thermal fluctuations, overlaps between atoms cannot be fully avoided. To treat such overlaps, in the third stage an energy minimisation procedure for all atoms is required.

We perform such a “global”, with respect to the number of atoms that are involved, minimisation scheme in two steps: first, the non-bonded interaction potential, between all UA groups, is switched off and the bonded (involving all atomistic bonds,

angles and dihedrals) potential is minimised through a steepest descent method, while the centers-of-mass corresponding to the CG beads A and B are restrained in their original positions. The improper dihedral potentials used to describe the tacticity of each polymer chain by fixing the tetrahedral configuration around the sp^3 -C connected to the phenyl ring are also involved in the minimisation scheme. Second, the non-bonded potential is switched on the restraints on center-of-masses are removed, and the full atomistic force field (all bonded and non-bonded interactions) is minimised *via* a conjugate gradient algorithm.

Short MD runs: finally, in order to relax remaining stresses in the systems and to obtain a realistic atomistic trajectory at the appropriate temperature, a short *NVT* MD run, of about 100 ps, is executed.

3.4.1 Validating backmapping of atomistic, low MW PS systems. The quantitative validation of the backmapping from the chemically specific CG model to the atomistic one is a challenging issue. Indeed, a direct comparison of the atomistic configurations of high MW polymer melts derived from the CG model with “reference” data is not possible, since in principle there are no accurate atomistic data for such polymer configurations.

Therefore, in order to validate the backmapping procedure we decide to use a low MW (1 kDa, 10mer) PS melt, at $T = 463$ K. First, we perform long atomistic MD simulations of atactic 10mer PS melts, using the model described in Section 2. These simulations are performed in the *NPT* ensemble, whereas tail corrections for the energy and pressure were applied. The integration time step was 1 fs, whereas the overall atomistic simulation time of the production runs was 100 ns.

Second, we apply the backmapping methodology, described in the previous section, to a CG 10mer PS system.¹⁴ Thus, we obtain atomistic configurations of 10mer PS without performing atomistic MD simulations.

Overall, for the low MW PS melt atomistic data are gathered both from long atomistic MD simulations (“reference” data) and from CG systems after employing the CG-to-atomistic backmapping procedure. As a direct “intramolecular” check of the backmapping process we examine the internal distance plot, analysed at the united-atom level, of a typical short-chain system (MW = 1 kDa), obtained both from long atomistic MD simulations and after backmapping of the CG configurations. This internal distance plot is defined setting in eqn (5) $R^2(s) \equiv R_{AT}^2(n)$ and $m \equiv n$, where $R_{AT}^2(n)$ is the average mean square distance between two carbon atoms of the atomistic PS chains. Accordingly, n is the number of carbon atoms in the chain backbone between these two atoms. Data are shown in Fig. 9. As we can see the agreement between the two sets of data is excellent for all internal distances. Note that a similar agreement has been found before for short PS chains following a different back mapping approach.⁷³

The short chain PS atomistic configurations obtained from the CG ones through the backmapping procedure can be further examined by calculating the atomistic pair distribution functions, $g_{AT}(r)$, and comparing them against the data derived directly from the long atomistic runs. Results are presented in Fig. 10(a) and (b). First, in Fig. 10(a) data for the intramolecular distribution function, $g_{intra,AT}(r)$, are shown. The agreement

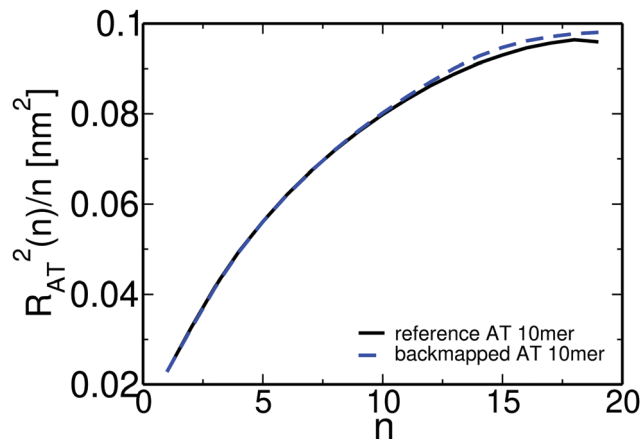


Fig. 9 Internal distance distribution, analysed at the united-atom level, of a typical system (MW = 1 kDa), obtained from long atomistic MD simulations and after backmapping of the CG configurations.

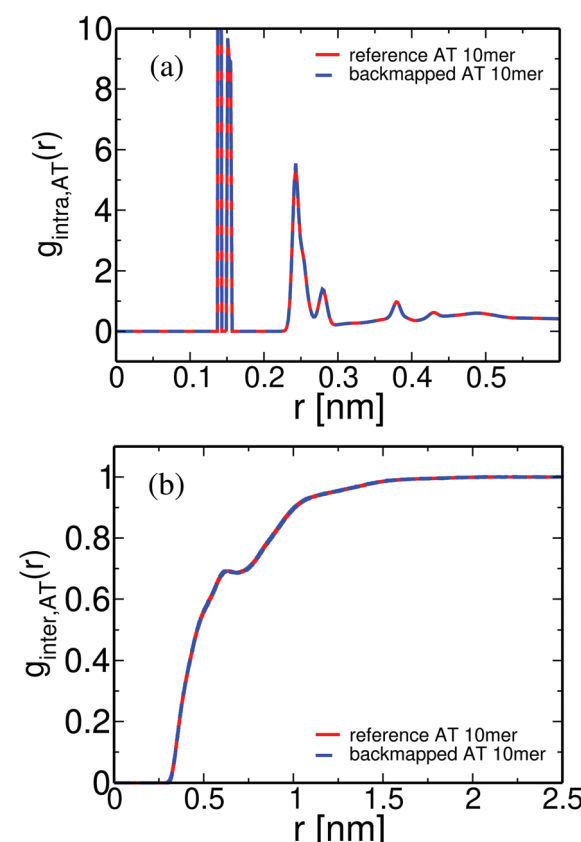


Fig. 10 (a) Intramolecular and (b) intermolecular pair distribution functions for a PS melt (MW = 1 kDa, $T = 463$ K), obtained from long atomistic MD simulations, and after backmapping of the CG configurations.

between the two curves is excellent for all length scales, providing thus direct evidence of the applicability of the coarse-grained model to preserve the long length internal chain structure. Note that these data include all intramolecular correlations, in contrast to the internal distance distribution data shown in Fig. 9, where only correlations along the backbone atoms are considered. Thus the agreement between the two sets of data shown in Fig. 10(a)

proves the ability of the backmapping methodology to reproduce the full intramolecular structure.

The intermolecular pair distribution function, $g_{\text{inter,AT}}(r)$, is shown in Fig. 10(b). The excellent agreement between the two different sets of data clearly demonstrates that the local packing in the backmapped atactic PS melts is also well reproduced. Note that the agreement between the intermolecular distribution functions based on different correlations, *e.g.* of “CH₂–CH₂” and of “phenyl–phenyl” groups (data not shown here) is of similar quality.

3.4.2 High MW atomistic PS melts. After validating the “CG-to-atomistic” backmapping methodology we can proceed to applying this approach to the high MW (50 kDa) CG PS melts, which have been obtained through the “blobs-to-CG” backmapping procedure described in Section 3.2. By doing this, atomistic conformations of 480mer (MW = 50 kDa) PS melts are directly obtained. Such well equilibrated high MW atomistic PS configurations cannot be generated through brute force MD simulations, even with the most powerful computing resources.

A typical well-equilibrated atomistic configuration (snapshot) of a 50 kDa PS melt with 100 chains is shown in Fig. 11.

The structure of polymeric chains, and its dependence on the molecular weight, is of special importance. Thus, in the following we compare the pair distribution functions of the long (entangled) PS chains with the data from the short (oligomeric) PS discussed above. The structure of the derived atomistic PS 480mer configuration is examined in Fig. 12(a) and (b). In Fig. 12(a) data for the atomistic intramolecular distribution function, $g_{\text{intra,AT}}(r)$ of both low (10mer) and high (480mer) molecular weight PS melts are shown. The agreement between the two curves at very short distances of about 0.5 nm is expected. Indeed, correlations on such length scales involve neighboring

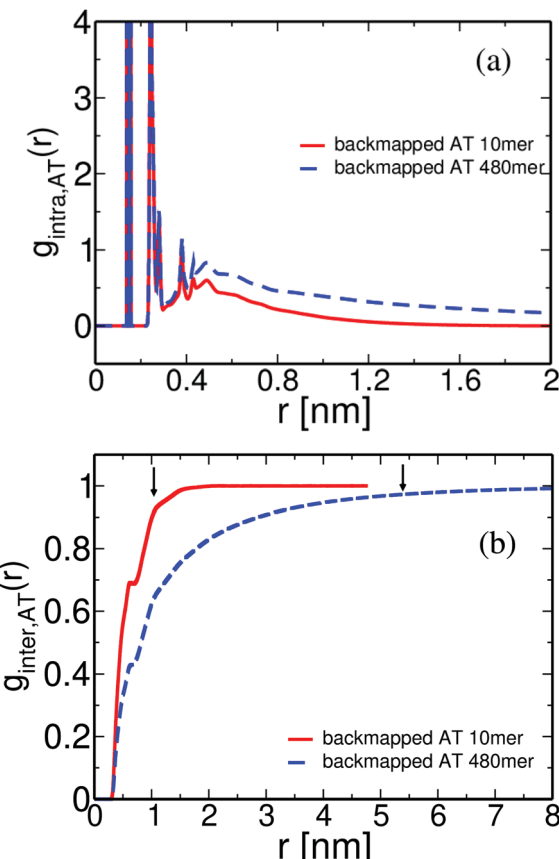


Fig. 12 (a) Intramolecular and (b) intermolecular pair distribution functions for different PS melts, obtained directly from backmapping of the CG configurations. Arrows denote the average radius of gyration of the chains for both systems, $R_g(1 \text{ kDa}) = 0.9 \text{ nm}$ and $R_g(50 \text{ kDa}) = 5.4 \text{ nm}$.

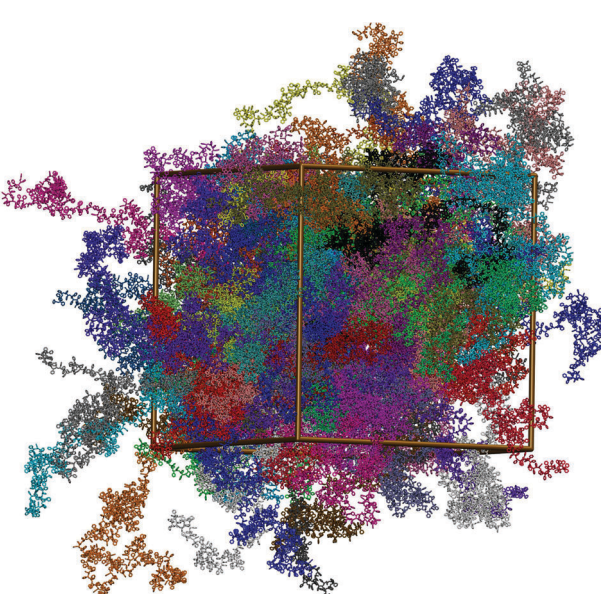


Fig. 11 Equilibrated atomistic configuration of a 50 kDa (480mer) PS melt with 100 chains ($T = 463 \text{ K}$). Chains are shown unwrapped (with the center-of-mass of each chain in the simulation box) and with different colors for clarity.

atoms along the polymer chain (*i.e.* atoms belonging only to one or two consecutive monomers), thus being very similar for the low and high molecular weight chains. At greater distances intramolecular distribution functions approach zero, as expected; however, $g_{\text{intra,AT}}(r)$ for 480mer PS chains is extended to much longer lengths.

Different is the case for the overall chain packing, which is directly related to the correlation hole of the polymer chains.¹⁸ Data about the intermolecular pair distribution function, $g_{\text{inter,AT}}(r)$, are shown in Fig. 12(b). It is obvious that the correlation hole extends over a distance of the order of the average radius of gyration of the chains; the latter is shown, for both systems, in Fig. 12(b) with arrows. In addition, for the high molecular weight chains the correlation hole becomes less deep, as has been also discussed before.⁴⁹

We present in Fig. 13 the internal distance plot $R_{\text{AT}}^2(n)/n$ calculated for one representative backmapped sample of an atomistic 50 kDa PS melt (solid black line). $R_{\text{AT}}^2(n)$ stands for the average mean square distance between n consecutive backbone carbon atoms of the atomistic PS chains. For comparison, the internal distance plot calculated for the sample of the moderately CG melt used to backmap this atomistic sample is also shown (dashed red line). For the atomistic sample, the

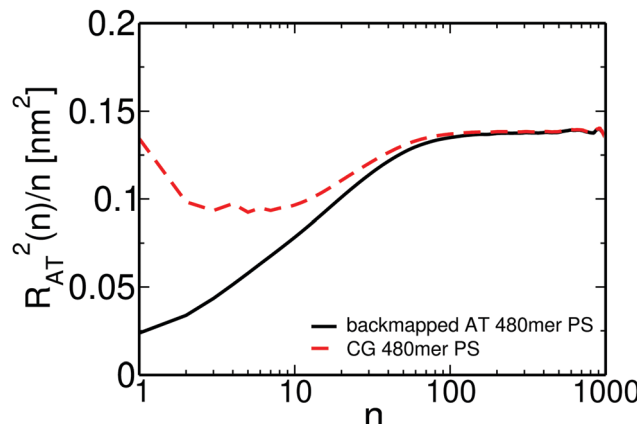


Fig. 13 Internal distance distribution, analysed at the united-atom level, of a high MW PS chain obtained directly after backmapping of the CG configurations, without performing long atomistic MD runs.

internal distances start from a small value and then smoothly reach a plateau for n around 80–100, which corresponds to 40–50 PS monomers. This behavior at small n differs from the internal distance plot in the moderately CG representation, where $R_{AT}^2(n)/n$ appears non-monotonous and more structured. Such differences are expected because of the averaging of the monomeric degrees of freedom performed in the CG groups. In contrast, the two plots match each other at large n , demonstrating that our “CG-to-atomistic” backmapping procedure conserves the global conformational properties that have already been equilibrated during the “blob-to-CG” backmapping stage.

4 Conclusions and outlook

In this work, we propose a method for efficiently generating well-equilibrated configurations of high molecular-weight polymer melts, described with chemically-specific atomistic models. The method is build on a hierarchy of models, which describe the same material with different resolutions: from mesoscopic to atomistic. The modelling hierarchy includes a soft blob-based, a moderately coarse-grained, and an atomistic model. If required, more soft blob-based models can be incorporated to accelerate equilibration of larger scales. Each model in the hierarchy is parameterised to reproduce key conformational and structural properties characterising the melt, when described with the next finer-resolution model. First, the melt is efficiently equilibrated using the soft blob-based model. The details of the next level are reinserted, the system is re-equilibrated, and we proceed to the next reinsertion step. During each step of backmapping only local re-equilibration is required. Therefore, the computation time is independent of the molecular weight of the polymer that is considered.

The hierarchical backmapping method presented in this study aims to deliver well-equilibrated atomistically-resolved configurations of highly entangled polymer melts. Preparing such configurations *via* hierarchical backmapping circumvents the major bottleneck of equilibration schemes with realistic

dynamics – the need to address time-scales larger than the reptation time, τ_{rep} ; *i.e.* the problem of long relaxation times. The backmapped atomistic configurations derived here are conceived to serve as an input for further computational studies of structural, dynamical and rheological properties, in and out of equilibrium. For the latter, the input configurations must be subjected to techniques such as standard non-equilibrium molecular dynamics (NEMD) and protracted computational times cannot be avoided. We emphasize, however, that many properties and phenomena relevant for polymer dynamics and rheology can be captured either from equilibrium MD simulations, *e.g.* using Green-Kubo relations for linear transport coefficients, or from NEMD simulations on time scales shorter than τ_{rep} ; in either case, nevertheless, equilibrated starting states are required. Such simulations can be costly computationally but already manageable with modern super-computers.^{51,74–79}

Finally, we mention that considering flow effects already on the level of blob-based models offers an interesting possibility. The blob-based model of our study cannot be used for a mesoscopic description of flow since it does not include a way to avoid crossings between polymer chains, which are allowed by the soft potentials. Methods for recovering non-crossability of chains in blob-based models are available, *e.g.* using phenomenological interactions (*e.g.* *via* slip-links^{80,81} or slip-springs^{82–85}) or algorithmic detection and prevention of intersections.^{15,36} Performing backmapping from such “rheologically-consistent” blob-based models is an interesting perspective for generating off-equilibrium all-atom configurations.

Overall, here, as a proof-of-concept, we use the proposed multi-resolution method to equilibrate atomistically-resolved samples of melts of long atactic polystyrene chains. The preparation of such systems using brute force MD simulations is unfeasible, even with modern supercomputers. We emphasise that the method is not restricted to polystyrene and can be straightforwardly applied to equilibrate melts of other polymeric materials, where moderately CG models exist.^{16,86–90}

Conflicts of interest

There are no conflicts to declare.

Appendix: “push-off” procedure for backmapping the blob-based model to the chemically specific coarse-grained model

The whole “push-off” procedure is accomplished in 100 cycles of a molecular dynamics simulation, where each cycle is comprised of 2×10^4 steps, and time step $\Delta t = 0.0001\tau$ (τ is the time unit in the CG PS model). (a) For all particle pairs ij other than the intramolecular (1,5) pairs $r_{c(n)}$ is linearly decreased from $0.9 r_{ij}^{cutoff}$ (r_{ij}^{cutoff} is the cutoff of the LJ-like potential between i and j particles) to $0.5 r_{ij}^{cutoff}$ within the first 80 cycles, after which particle overlaps for those pairs can be



successfully removed. (b) For the intramolecular (1,5) pairs, the corresponding force-capped radius, $r_{c(1,5)}$, is allowed to fluctuate (instead of decreasing linearly as in case (a)) to prevent large distortions of chain conformations. For this purpose, after each cycle, we quantify *via* I (see eqn (7) in Section 3.1) the deviation of the internal distance plot from the reference one. Before starting the next cycle we decrease (or increase) $r_{c(1,5)}$ by $0.01\sigma_{1-5}$ if the calculated I is negative (or positive). In this way, $r_{c(1,5)}$ can fluctuate within the first 80 simulation cycles. In the last 20 cycles it is reduced linearly to 0.5 $r_{(1,5)}^{\text{cutoff}}$.

Acknowledgements

The computing time granted by the John von Neumann Institute for Computing (NIC) on the supercomputer JURECA at Jülich Supercomputing Centre (JSC) is gratefully acknowledged. This work has been supported by the European Research Council (ERC) under the Seventh Framework Programme (FP7/2007–2013)/ERC Grant Agreement No. 340906-MOLPROCOMP. G. Zhang acknowledges the support from the National Natural Science Foundation of China (21873023). Open Access funding provided by the Max Planck Society.

References

- 1 A. Yu. Grosberg and A. R. Kokhlov, *Statistical Physics of Macromolecules*, AIP, New York, 1994.
- 2 M. Müller, *J. Stat. Phys.*, 2011, **145**, 967–1016.
- 3 J. Zhang, D. Mukherji and K. Ch. Daoulas, *Eur. Phys. J.: Spec. Top.*, 2016, **225**, 1423–1440.
- 4 R. Everaers, S. K. Sukumaran, G. S. Grest, C. Svaneborg, A. Sivasubramanian and K. Kremer, *Science*, 2004, **303**, 823–826.
- 5 *Physical Properties of Polymers Handbook*, ed. J. E. Mark, Springer, 2007.
- 6 M. Doi and S. F. Edwards, *The Theory of Polymer Dynamics*, Oxford University Press, Oxford, 1986.
- 7 T. Spyriouni, C. Tzoumanekas and D. N. Theodorou, *Macromolecules*, 2007, **40**, 3876–3885.
- 8 V. G. Mavrantzas, T. D. Boone, E. Zervopoulou and D. N. Theodorou, *Macromolecules*, 1999, **32**, 5072–5096.
- 9 K. Kremer and F. Müller-Plathe, *Mol. Simul.*, 2002, **28**, 729–750.
- 10 W. G. Noid, J. W. Chu, G. S. Ayton, V. Krishna, S. Izvekov, G. A. Voth, A. Das and H. C. Andersen, *J. Chem. Phys.*, 2008, **128**, 244114.
- 11 *Coarse-Graining of Condensed Phase and Biomolecular Systems*, ed. G. A. Voth, CRC Press, Boca Raton, 2009.
- 12 W. G. Noid, *J. Chem. Phys.*, 2013, **139**, 090901.
- 13 C. Peter and K. Kremer, *Soft Matter*, 2009, **5**, 4357–4366.
- 14 V. A. Harmandaris, D. Reith and N. F. A. van der Vegt, *Macromol. Chem. Phys.*, 2007, **208**, 2109–2120.
- 15 J. T. Padding and W. J. Briels, *J. Phys.: Condens. Matter*, 2011, **23**, 233101.
- 16 W. Tschöp, K. Kremer, J. Batoulis, T. Bürger and O. Hahn, *Acta Polym.*, 1998, **49**, 61–74.
- 17 W. Tschöp, K. Kremer, O. Hahn, J. Batoulis and T. Bürger, *Acta Polym.*, 1998, **49**, 75–79.
- 18 P. G. de Gennes, *Scaling Concepts in Polymer Physics*, Cornell University Press, Ithaca, New York, 1979.
- 19 R. Auhl, R. Everaers, G. S. Grest, K. Kremer and S. J. Plimpton, *J. Chem. Phys.*, 2003, **119**, 12718–12728.
- 20 L. A. Moreira, G. J. Zhang, F. Müller, T. Stuehn and K. Kremer, *Macromol. Theory Simul.*, 2015, **24**, 419–431.
- 21 P. Carbone, H. A. Karimi-Varzaneh and F. Müller-Plathe, *Faraday Discuss.*, 2010, **144**, 25–42.
- 22 Y. R. Slizberg, M. Kröger and T. L. Chantawansri, *J. Chem. Phys.*, 2016, **144**, 154901.
- 23 J. P. Wittmer, P. Beckrich, H. Meyer, A. Cavallo, A. Johner and J. Baschnagel, *Phys. Rev. E: Stat., Nonlinear, Soft Matter Phys.*, 2007, **76**, 011803.
- 24 J. Glaser, J. Qin, P. Medapuram and D. C. Morse, *Macromolecules*, 2014, **47**, 851–869.
- 25 H. Meyer, E. Horwath and P. Virnau, *ACS Macro Lett.*, 2018, **7**, 757–761.
- 26 B. Steinmüller, M. Müller, K. R. Hambrecht, G. D. Smith and D. Bedrov, *Macromolecules*, 2011, **45**, 1107–1117.
- 27 G. J. Zhang, L. A. Moreira, T. Stuehn, K. Ch. Daoulas and K. Kremer, *ACS Macro Lett.*, 2014, **3**, 198–203.
- 28 D. Ozog, J. McCarty, G. Gossett, A. D. Malony and M. Guenza, *J. Comput. Sci.*, 2015, **9**, 33–38.
- 29 C. Svaneborg, H. A. Karimi-Varzaneh, N. Hojdis, F. Fleck and R. Everaers, *Phys. Rev. E*, 2016, **94**, 032502.
- 30 A. J. Parker and J. Rottler, *Macromol. Theory Simul.*, 2014, **23**, 401–409.
- 31 V. Sethuraman, S. Mogurampelly and V. Ganesan, *Macromolecules*, 2017, **50**, 4542–4554.
- 32 M. Laso, H. C. Öttinger and U. W. Suter, *J. Chem. Phys.*, 1991, **95**, 2178–2182.
- 33 M. Murat and K. Kremer, *J. Chem. Phys.*, 1998, **108**, 4340–4348.
- 34 C. Likos, *Phys. Rep.*, 2001, **348**, 267–439.
- 35 P. G. Bolhuis, A. A. Louis, J. P. Hansen and E. J. Meijer, *J. Chem. Phys.*, 2001, **114**, 4296–4311.
- 36 J. T. Padding and W. J. Briels, *J. Chem. Phys.*, 2001, **115**, 2846–2859.
- 37 F. Eurich and P. Maass, *J. Chem. Phys.*, 2001, **114**, 7655–7668.
- 38 V. Krakoviack, J.-P. Hansen and A. A. Louis, *Phys. Rev. E: Stat., Nonlinear, Soft Matter Phys.*, 2003, **67**, 041801.
- 39 T. Vettorel, G. Besold and K. Kremer, *Soft Matter*, 2010, **6**, 2282–2292.
- 40 A. J. Clark, J. McCarty, I. Y. Lyubimov and M. G. Guenza, *Phys. Rev. Lett.*, 2012, **109**, 168301.
- 41 R. Menichetti and A. Pelissetto, *J. Chem. Phys.*, 2013, **138**, 124902.
- 42 G. D'Adamo, A. Pelissetto and C. Pierleoni, *J. Chem. Phys.*, 2013, **138**, 234107.
- 43 G. J. Zhang, K. Ch. Daoulas and K. Kremer, *Macromol. Chem. Phys.*, 2013, **214**, 214–224.
- 44 A. Narros, C. N. Likos, A. J. Moreno and B. Capone, *Soft Matter*, 2014, **10**, 9601–9614.



45 G. D'Adamo, R. Menichetti, A. Pelissetto and C. Pierleoni, *Eur. Phys. J.: Spec. Top.*, 2015, **224**, 2239–2267.

46 D. Yang and Q. Wang, *J. Chem. Phys.*, 2015, **142**, 054905.

47 G. J. Zhang, T. Stuehn, K. Ch. Daoulas and K. Kremer, *J. Chem. Phys.*, 2015, **142**, 221102.

48 T. Ohkuma, K. Kremer and K. Daoulas, *J. Phys.: Condens. Matter*, 2018, **30**, 174001.

49 V. A. Harmandaris and K. Kremer, *Macromolecules*, 2009, **42**, 791–802.

50 V. A. Harmandaris and K. Kremer, *Soft Matter*, 2009, **5**, 3920–3926.

51 C. Baig and V. A. Harmandaris, *Macromolecules*, 2010, **43**, 3156–3160.

52 C. D. Wick, M. G. Martin and J. I. Siepmann, *J. Phys. Chem. B*, 2000, **104**, 8008–8016.

53 V. A. Harmandaris, N. Adhikari, N. F. A. van der Vegt and K. Kremer, *Macromolecules*, 2006, **39**, 6708–6719.

54 C. Liu, K. Kremer and T. Bereau, *Adv. Theory Simul.*, 2018, **1**, 1800024.

55 P. J. Flory, *J. Chem. Phys.*, 1949, **17**, 303–310.

56 D. Lhuillier, *J. Phys.*, 1988, **49**, 705–710.

57 In previous implementations of the soft sphere model the prefactor N_b was adsorbed into c_2 . Here it appears explicitly in the term $c_2 N_b^2 / \sigma^3$ (see eqn (2)) to highlight the relevance to the Flory free energy.

58 In previous implementations of the soft sphere model the prefactor N_b^2 was adsorbed into ε .

59 R. L. C. Akkermans and W. J. Briels, *J. Chem. Phys.*, 2001, **114**, 1020–1031.

60 Q. Wang and D. Yang, *Polymer*, 2017, **111**, 103–106.

61 M. Dinpajoooh and M. G. Guenza, *Polymer*, 2017, **117**, 282–286.

62 G. Fleisher, *Colloid Polym. Sci.*, 1987, **265**, 89–95.

63 M. Antonietti, K. J. Fölsch and H. Sillescu, *Makromol. Chem.*, 1987, **188**, 2317–2324.

64 L. J. Fetters, D. L. Lohse, D. Richter, T. A. Witten and A. Zirkel, *Macromolecules*, 1994, **27**, 4639–4647.

65 A. P. Lyubartsev and A. Laaksonen, *Phys. Rev. E: Stat. Phys., Plasmas, Fluids, Relat. Interdiscip. Top.*, 1995, **52**, 3730–3737.

66 F. Müller-Plathe, *ChemPhysChem*, 2002, **3**, 754–769.

67 H.-P. Hsu and K. Kremer, *J. Chem. Phys.*, 2016, **144**, 154907.

68 J. D. Halverson, T. Brandes, O. Lenz, A. Arnold, S. Bevc, V. Starchenko, K. Kremer, T. Stuehn and D. Reith, *Comput. Phys. Commun.*, 2013, **184**, 1129–1149.

69 R. S. Graham, A. E. Likhtman and T. C. B. McLeish, *J. Rheol.*, 2003, **47**, 1171–1200.

70 J. E. Mark, *Physical Properties of Polymers Handbook*, Springer, 2nd edn, 2007.

71 L. E. Lombardi, M. A. Martí and L. Capece, *Bioinformatics*, 2016, **32**, 1235–1237.

72 G. Santangelo, A. Di Matteo, F. Müller-Plathe and G. Milano, *J. Phys. Chem. B*, 2007, **111**, 2765–2773.

73 D. Fritz, V. A. Harmandaris, K. Kremer and N. F. A. van der Veg, *Macromolecules*, 2009, **42**, 7579–7588.

74 J. Ramos, J. F. Vega, D. N. Theodorou and J. Martinez-Salazar, *Macromolecules*, 2008, **41**, 2959–2962.

75 J.-X. Hou, C. Svaneborg, R. Everaers and G. S. Grest, *Phys. Rev. Lett.*, 2010, **105**, 068301.

76 H. P. Hsu and K. Kremer, *ACS Macro Lett.*, 2018, **7**, 107–111.

77 H. P. Hsu and K. Kremer, *Phys. Rev. Lett.*, 2018, **121**, 167801.

78 S. Jeong, J. M. Kim and C. Baig, *Macromolecules*, 2017, **50**, 3424–3429.

79 M. Kröger and S. Hess, *Phys. Rev. Lett.*, 2000, **85**, 1128–1131.

80 A. E. Likhtman, *Macromolecules*, 2005, **38**, 6128–6139.

81 D. M. Nair and J. D. Schieber, *Macromolecules*, 2006, **39**, 3386–3397.

82 Y. Masubuchi, J. I. Takimoto, K. Koyama, G. Ianniruberto, G. Marrucci and F. Greco, *J. Chem. Phys.*, 2001, **115**, 4387–4394.

83 J. Oberdisse, G. Ianniruberto, F. Greco and G. Marrucci, *Rheol. Acta*, 2006, **46**, 95–109.

84 Y. Masubuchi, T. Uneyama, H. Wanatabe, G. Ianniruberto, F. Greco and G. Marrucci, *J. Chem. Phys.*, 2010, **132**, 134902.

85 V. Chappa, D. Morse, A. Zippelius and M. Müller, *Phys. Rev. Lett.*, 2012, **109**, 148302.

86 B. Hess, S. León, N. F. A. van der Vegt and K. Kremer, *Soft Matter*, 2006, **2**, 409–414.

87 T. Ohkuma and K. Kremer, *Polymer*, 2017, **130**, 88–101.

88 Y. N. Pandey, A. Brayton, C. Burkhart, G. J. Papakonstantopoulos and M. Doxastakis, *J. Chem. Phys.*, 2014, **140**, 054908.

89 Q. Sun and R. Faller, *J. Chem. Phys.*, 2007, **126**, 144908.

90 C. A. Lemarchand, M. Couty and B. Rousseau, *J. Chem. Phys.*, 2017, **146**, 074904.

